Physics of Fluids

Electrokinetic instability in microchannel viscoelastic fluid flows with conductivity gradients

Cite as: Phys. Fluids **31**, 082001 (2019); https://doi.org/10.1063/1.5105387
Submitted: 27 April 2019 . Accepted: 13 July 2019 . Published Online: 02 August 2019

Le Song (宋乐), Purva Jagdale, Liandong Yu (于连栋), Zhijian Liu (刘志坚), Di Li (李迪), Cheng Zhang (章诚), and Xiangchun Xuan (宣向春)

Physics of Fluids ARTICLE scitation.org/journal/phf

Electrokinetic instability in microchannel viscoelastic fluid flows with conductivity gradients

Cite as: Phys. Fluids 31, 082001 (2019); doi: 10.1063/1.5105387
Submitted: 27 April 2019 • Accepted: 13 July 2019 •
Published Online: 2 August 2019

Le Song (宋乐),[1,2,a)] Purva Jagdale,[2,a)] Liandong Yu (于连栋),[1,b)] Zhijian Liu (刘志坚),[2,3] Di Li (李迪),[2] Cheng Zhang (章诚),[4] and Xiangchun Xuan (宣向春)[2,b)]

AFFILIATIONS

[1]School of Instrument Science and Opto-Electronic Engineering, Hefei University of Technology, Hefei 230009, China
[2]Department of Mechanical Engineering, Clemson University, Clemson, South Carolina 29634-0921, USA
[3]College of Marine Engineering, Dalian Maritime University, Dalian 116026, China
[4]Department of Mechanical Engineering, University of West Florida, Pensacola, Florida 32514, USA

[a)]**Contributions:** L. Song and P. Jagdale contributed equally to this work.
[b)]**Authors to whom correspondence should be addressed:** liandongyu@hfut.edu.cn and xcxuan@clemson.edu.

ABSTRACT

Electrokinetic instability (EKI) is a flow instability that occurs in electric field-mediated microfluidic applications. It can be harnessed to enhance sample mixing or particle trapping but has to be avoided in particle separation. Current studies on EKI have been focused primarily on the flow of Newtonian fluids. However, many of the chemical and biological solutions exhibit non-Newtonian characteristics. This work presents the first experimental study of the EKI in viscoelastic fluid flows with conductivity gradients through a T-shaped microchannel. We find that the addition of polyethylene oxide (PEO) polymer into Newtonian buffer solutions alters the threshold electric field for the onset of EKI. Moreover, the speed and temporal frequency of the instability waves are significantly different from those in the pure buffer solutions. We develop a three-dimensional preliminary numerical model in COMSOL, which considers the increased viscosity and conductivity as well as the suppressed electroosmotic flow of the buffer-based PEO solutions. The numerically predicted threshold electric field and wave parameters compare favorably with the experimental data except at the highest PEO concentration. We attribute this deviation to the neglect of fluid elasticity effect in the current model that increases with the PEO concentration.

I. INTRODUCTION

Electrokinetic instability (EKI) is a flow instability observed in the development of electric field-mediated microfluidic applications.[1] It is induced by an electric body force, $\mathbf{f}_e$, that results from the interaction of electric field and fluid property gradients[2]

$$\mathbf{f}_e = \rho_e \mathbf{E} - \frac{1}{2}(\mathbf{E}\cdot\mathbf{E})\nabla\varepsilon, \tag{1}$$

where ρ_e is the free charge density, $\mathbf{E}$ is the electric field, and ε is the permittivity of the fluid that is assumed incompressible here. The two terms on the right-hand side of Eq. (1) represent the Coulomb and dielectric forces, respectively. Making use of Gauss' law, $\nabla\cdot(\varepsilon\mathbf{E}) = \rho_e$, and the conservation equation for current, $\nabla\cdot(\sigma\mathbf{E}) = 0$, one can readily obtain[3]

$$\rho_e = -\varepsilon\mathbf{E}\cdot\frac{\nabla\sigma}{\sigma} + \mathbf{E}\cdot\nabla\varepsilon, \tag{2}$$

where σ is the electric conductivity of the fluid. Therefore, the action of electric field on a fluid with a nonuniform electric conductivity or permittivity generates a body force in the direction of either the electric field or the property gradient, which, if strong enough, may cause EKI.[1]

The spatial variation of fluid properties occurs inherently at the interface of two fluids that are displacing[4] or coflowing with[5] each other. The former situation takes place in both the field amplified sample stacking via isotachophoresis[6] and the measurement

of electroosmotic flow via current monitoring,[7] where the applied electric field is collinear with the fluid property gradient. The electrokinetic co-flow of two (or more) fluids with dissimilar properties takes place in microfluidic mixing[8–10] and sheath focusing-based particle separation,[11–13] where the electric field is orthogonal to the fluid property gradient at the base state. Strong EKI can be induced in this situation even if the Reynolds number is low,[14–18] which has been utilized for microfluidic mixing applications.[19–21] The effects of various parameters, including electric field,[22,23] fluid properties,[24–26] channel configuration,[27–29] channel dimension,[30,31] and multiple species[32] have been systematically investigated. The spatial variation of fluid properties also occurs in the electroosmotic flow of single fluids if the fluid temperature becomes nonuniform as a consequence of the ubiquitous Joule heating effects.[33,34] This is attributed to the strong temperature dependence of the fluid conductivity and permittivity.[35] The electric field may be at various angles with respect to the local temperature-induced fluid property gradients, which has been reported to cause electrothermal circulations in insulator-based dielectrophoretic microdevices.[36,37]

In addition, EKI may be induced by a similar electric body force to that in Eq. (1), which, however, results from the action of electric field upon the free charge density inside the electric double layer (EDL) formed spontaneously at the (homogeneous) fluid-solid interface (i.e., the microchannel walls).[38] As the EDL thickness is typically very thin as compared to the characteristic dimension of microfluidic channels,[39] this electric force becomes essentially a surface force and is often considered via an electroosmotic slip velocity, U_{slip}, on an otherwise nonslip channel wall[40]

$$U_{slip} = -\frac{\varepsilon\zeta}{\mu}\mathbf{E}\cdot\mathbf{t}, \tag{3}$$

where ζ is the wall zeta potential, μ is the fluid viscosity, and $\mathbf{t}$ is the unit tangential vector of the wall. Therefore, the discontinuity of U_{slip} on any channel walls may lead to local disturbances to the otherwise pluglike electroosmotic fluid flow.[41] This EKI has been reported to occur when the wall surface charge varies spatially as a result of the heterogeneous patterning,[42] field effect control,[43] or induced charge effect.[33,44–47] The resulting fluid circulations[48,49] have been demonstrated to enhance sample mixing[50,51] and particle trapping[52,53] in several microfluidic applications.

However, all studies that are reviewed above have been focused on the electroosmotic flow of Newtonian fluids. As a matter of fact, many of the real chemical (e.g., polymer solutions and colloidal suspensions) and biological (e.g., blood and DNA solutions) solutions are complex fluids and exhibit non-Newtonian characteristics (e.g., elasticity and shear thinning).[54–57] It is therefore natural and important to ask if and how the fluid rheological properties may affect the EKI in microchannel flows. Previous studies on electroosmosis of non-Newtonian fluids and electrophoresis of particles therein have been mainly carried out theoretically or numerically,[58] many of which have yet to be experimentally validated. Among the few experimental studies in the literature, electro-elastic instabilities are reported in the flow of polyacrylamide (PAA) solutions (strongly elastic and strong shear thinning[59]) through both a constriction[60] and a cross-shaped microchannel.[61] Also, multiple pairs of circulations are observed in the electroosmotic flow of xanthan gum (XG) solutions (strongly shear thinning with little elasticity[62]) through a constriction microchannel.[63] Recently, our group has reported abnormal electrophoretic particle behaviors in polyethylene oxide (PEO) solutions (moderately elastic and weakly to mildly shear thinning[64]) through a constriction microchannel.[65,66] Moreover, our group has observed exactly opposite lateral particle migrations in the Poiseuille-electroosmotic flow of PEO solution as compared to those in a Newtonian fluid.[67] Such a reversed particle migration phenomenon has also been reported in the electroosmotic flow of XG solutions through a straight rectangular microchannel.[68]

We perform in this work the first experimental study on the electroosmotic coflow of viscoelastic fluids with distinct electric conductivities through a T-shaped microchannel. We use a range of buffer-based PEO solutions in the test with the aim to study how the fluid elasticity may affect the conductivity ratio-induced EKI. We also develop a three-dimensional (3D) numerical model to understand and predict the dynamic flow behaviors at the viscoelastic fluid interface. The numerical predictions of both the threshold electric field (for the onset of EKI) and the instability wave parameters (including the wave speed and the temporal frequency) are compared against the experimental measurements.

II. EXPERIMENT

A. Materials

Figure 1 shows a picture of the microfluidic chip used in the experiment. It contains a T-shaped microchannel that was fabricated using polydimethylsiloxane (PDMS) with the standard soft lithography technique. The detailed fabrication procedure can be referred to our earlier work.[24] The two side-branches of the microchannel are each 8 mm long and 100 μm wide, and the main-branch is 10 mm long and 200 μm wide. The depth of the microchannel measures 67 μm. Two 1 ml pipette tips were inserted into the holes of the side-branches to serve as the inlet reservoirs, where Inlets 1 and 2 (Fig. 1) were filled with 2.0 mM and 0.2 mM phosphate buffer solutions, respectively. PEO powder ($M_w = 2 \times 10^6$ Da, Sigma-Aldrich) was dissolved into each solution at an equal amount, whose final concentration was varied from 0 (i.e., Newtonian) to 1000 ppm (i.e., non-Newtonian or viscoelastic). These concentrations are all smaller

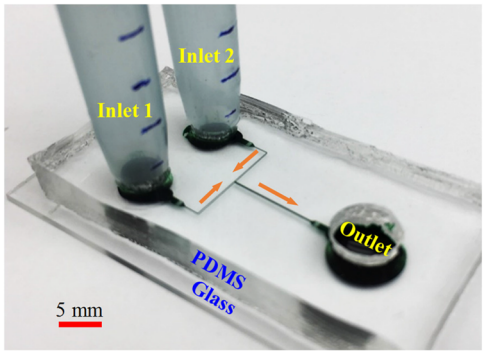

FIG. 1. Picture of the microfluidic chip used in the experiment. The two pipette tips (with height markings) serve as the inlet reservoirs for producing an equal pressure-driven flow in the two side-branches of the T-shaped microchannel, which is concurrent with the DC electric field (imposed across the electrodes inserted into the liquids in the inlet and outlet reservoirs) driven fluid flow.

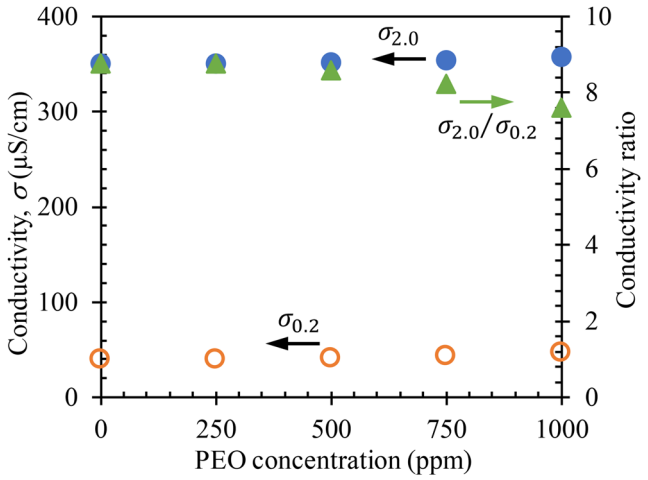

FIG. 2. Experimentally measured electric conductivities of 2.0 mM ($\sigma_{2.0}$, filled circles) and 0.2 mM ($\sigma_{0.2}$, hollow circles) buffer-based PEO solutions. The calculated conductivity ratio (filled triangles), $\sigma_{2.0}/\sigma_{0.2}$, of these two solutions decreases slowly with the increase in the PEO concentration.

than the overlapping concentration, $c^* = 0.77/[\eta] = 858$ ppm of the PEO polymer except for 1000 ppm, where $[\eta] = 0.072M_w^{0.65} = 897$ ml/g is the intrinsic viscosity.[69] Therefore, our prepared PEO solutions are in the dilute (≤750 ppm) or semidilute (1000 ppm) regime, and thus each has a moderate elasticity and a weak shear thinning.[69] The 2.0 mM buffer-based PEO solution at inlet 1 was also mixed with 50 μM rhodamine B dye (Sigma-Aldrich) for visualizing the interfacial behavior between the two fluids.

Figure 2 shows the measured electric conductivity values (Fisher Scientific, Accumet AP85) of the prepared buffer/PEO solutions (in the absence of the rhodamine B dye). The addition of PEO appears to increase slightly the conductivity values of both buffer-based solutions. However, the extent of this increase becomes non-negligible for the 0.2 mM buffer-based PEO solution because of the small conductivity of the buffer solution itself. Consequently, the conductivity ratio of 2.0 mM–0.2 mM buffer-based PEO solutions decreases gradually from 8.8 at 0 ppm PEO to 7.6 at 1000 ppm (Fig. 2). We also measured the electric conductivity of a couple of dyed PEO solutions in 2.0 mM buffer and found no significant differences with or without the dye. The zero-shear-rate viscosities of the prepared solutions are listed in Table I. They were assumed to be only dependent on the PEO concentration regardless of the buffer concentration. The viscosity values of 500 ppm and 1000 ppm PEO solutions were extracted from the experimental data of Rodd *et al.*[69] Those of 250 ppm and 750 ppm were calculated using the viscosity blending equation.[70]

The average zeta potential of the hybrid PDMS/glass channel walls was measured by tracking the front of neutral rhodamine B dye in the electroosmotic flow of each prepared solution through a 2 cm long straight rectangular microchannel. This channel (along with the two reservoirs) was fabricated using exactly the same procedure as the T-shaped microchannel to ensure the consistency of the wall properties. It was first filled with a buffer or a buffer-based PEO solution, where the liquid heights at the inlet and outlet reservoirs were balanced to minimize the pressure-driven flow. Then, the solution at the inlet reservoir was replaced with an equal volume of the same solution but mixed with 50 μM rhodamine B dye. The front of the dye solution was tracked after a DC electric field was imposed upon the channel right away. The electroosmotic flow velocity was determined by dividing the travel distance of the dye front over the travel time, with which the zeta potential could be roughly estimated using the Smoluchowski equation, i.e., Eq. (3).[39,40] The obtained zeta potential values are −23 mV and −46 mV for the 2.0 mM and 0.2 mM pure buffer solutions, respectively. We adopt the following approximate empirical correlation[14,15] to account for the dependence of the wall zeta potential, ζ, on the buffer concentration, c_b,

$$\zeta = \zeta_r C_b^{-0.3}, \tag{4}$$

where $C_b = c_b/c_r$ is the normalized buffer concentration with $c_r = 2.0$ mM being the reference concentration and $\zeta_r = -23$ mV is the reference zeta potential when $C_b = 1$ (i.e., $c_b = c_r$). The zeta potential of each of the buffer-based PEO solutions was found much smaller than that of the pure buffer solution and hence was assumed to be zero in our model.

TABLE I. Viscosity values of the prepared buffer-based PEO solutions.[69,70]

PEO concentration (ppm)	0	250	500	750	1000
Fluid viscosity μ (mPa s)	1.0	1.3	1.8	2.0	2.3

B. Methods

Platinum electrodes were inserted into the liquids in both the inlet and outlet reservoirs. Those at the inlet reservoirs were connected to a high-voltage DC power supply (Glassman High Voltage, Inc.) in parallel, while the electrode at the outlet was grounded. Such a setup generated an equal DC electric field through each of the side-branches of the T-shaped microchannel. As the electroosmotic flow of buffer-based PEO solutions was found very weak in our experiments, a concurrent pressure-driven flow was introduced to pump the viscoelastic solutions through the microchannel. This was implemented simply by raising the liquid heights in the two pipette tips (Fig. 1). Note that the liquid heights at the inlet reservoirs were kept leveled in every test, whose value relative to that at the outlet reservoir (read from the markings on the pipette tips) was varied from 0 to 1.5 cm to generate an equal pressure-driven flow in the two side-branches at varying flow rates. The dynamic fluid behavior at the T-junction of the microchannel was visualized and recorded using an inverted fluorescent microscope (Nikon Eclipse TE2000U, Nikon Instruments) along with a CCD camera (Nikon DS-Qi1Mc) at a rate of 15 frames per second. The obtained videos and images were postprocessed using the Nikon imaging software (NIS-Elements AR 2.30).

III. THEORY

A. Governing equations

A 3D numerical model was developed to understand and simulate the electrohydrodynamic microchannel flow of viscoelastic fluids with conductivity gradients. As a preliminary study, we ignored

the elasticity effect of the PEO solution and considered only its influence on the fluid viscosity (Table I), conductivity (Fig. 1), and wall zeta potential (see Sec. II). Referring to previous works on EKI in Newtonian fluids from the Santiago group,[14,15] we solved the following conservation equations for charged species, current, mass, and momentum, respectively,

$$\frac{\partial \sigma}{\partial t} + \mathbf{u} \cdot \nabla \sigma = D \nabla^2 \sigma, \tag{5}$$

$$\nabla \cdot (\sigma \nabla \phi) = 0, \tag{6}$$

$$\nabla \cdot \mathbf{u} = 0, \tag{7}$$

$$\rho\left(\frac{\partial \mathbf{u}}{\partial t} + \mathbf{u} \cdot \nabla \mathbf{u}\right) = -\nabla p + \mu \nabla^2 \mathbf{u} + \varepsilon\left(\nabla^2 \phi\right) \nabla \phi, \tag{8}$$

where $\sigma = \sigma_{2.0} C_b + \sigma_{0.2}(1 - C_b)$ is the buffer concentration (note $0 \le C_b \le 1$) dependent fluid conductivity with $\sigma_{2.0}$ and $\sigma_{0.2}$ being the conductivities of the 2.0 mM and 0.2 mM buffer-based PEO solutions (see Fig. 1), t is the time coordinate, $\mathbf{u}$ is the fluid velocity, $D = D_0 \mu_0 / \mu$ is the diffusion coefficient of the buffer ions with $D_0 = 1 \times 10^{-9}$ m^2/s assumed as the diffusivity in the pure buffer solutions of viscosity μ_0 (i.e., at 0 ppm PEO; see Table I), ϕ is the electric potential with the electric field given by $\mathbf{E} = -\nabla\phi$, $\rho = 1000$ kg/m^3 is the fluid density, p is the pressure, and $\varepsilon = 7.083 \times 10^{-10}$ C^2/J·m is the fluid permittivity that is assumed equal to that of water. Note that other than the electric conductivity, all other fluid properties including density, viscosity, and permittivity were assumed uniform in between the two buffer-based PEO solutions in our model. This assumption has been often used in the numerical models for EKI in Newtonian fluids in the literature.[22–32] It is supposed to still remain valid in our system because an equal concentration of PEO is added to each buffer solution. The influence of the addition of rhodamine B dye on the fluid properties was assumed negligible in our model.

We also solved an advection-diffusion equation to simulate the behavior of neutral rhodamine B dye for a direct comparison with the experimental observation,

$$\frac{\partial C_d}{\partial t} + \mathbf{u} \cdot \nabla C_d = D_d \nabla^2 C_d, \tag{9}$$

where C_d is the dimensionalized (by its original 50 μM concentration) dye concentration and $D_d = D_{d0}\mu_0/\mu$ is the diffusion coefficient of the dye molecules with $D_{d0} = 3 \times 10^{-11}$ m^2/s being the assumed diffusivity[14,15] in the pure buffer solutions (i.e., at 0 ppm PEO). It is important to note that the governing equations, Eqs. (5)–(8), are coupled through the fluid conductivity and need to be solved simultaneously in the model. In contrast, the dye concentration in Eq. (9) is decoupled from the other fields and hence can be considered after the other governing equations have all been solved. We note that electroosmotic flow has been reported to exhibit a hysteresis in the situations where two fluids with difference concentrations are displacing one another.[71,72] We are unsure if such an effect also occurs in our system where the two dissimilar fluids are coflowing with each other. We will defer this study to our future work.

B. Model implementations

Figure 3 shows the computational domain of our 3D model, which is meshed with free tetrahedral elements. It also highlights the important boundary conditions for the governing equations, which are summarized in the follows. For the buffer conductivity field in Eq. (5), the inlets 1 and 2 are imposed with $\sigma = \sigma_{2.0}$ and $\sigma = \sigma_{0.2}$, respectively; all other surfaces are assumed nonpenetrating (the channel walls) or fully developed (the outlet), i.e., $\nabla\sigma \cdot \mathbf{n} = 0$ with $\mathbf{n}$ being the unit normal vector. For the electric (potential) field in Eq. (6), the two inlets are imposed with an equal electric potential, $\phi = \phi_{in}$, and the outlet is grounded. All channel walls are electrically insulated, $\nabla\phi \cdot \mathbf{n} = 0$. For the flow field in Eqs. (7) and (8), the channel walls are imposed with the electroosmotic slip velocity in Eq. (3), i.e., $\mathbf{u} \cdot \mathbf{t} = U_{slip}$. The inlets 1 and 2 are imposed with an equal hydrostatic pressure that is converted from the liquid height difference between the inlet and outlet reservoirs, and the outlet is assigned a zero pressure. For the dye concentration field in Eq. (9), the inlets 1 and 2 are imposed with $C_d = 1$ and $C_d = 0$, respectively; all other surfaces are nonpenetrating with $\nabla C_d \cdot \mathbf{n} = 0$. At the initial state, the two fluids from the inlets 1 and 2 are both assumed stationary with a uniform but distinct conductivity in each half of the computation domain. The dye concentration also has a uniform value in each half domain.

Our model was developed and solved in COMSOL® 5.3. A grid-independence study was performed to ensure the model accuracy, where the smallest mesh size was varied from 8 μm to

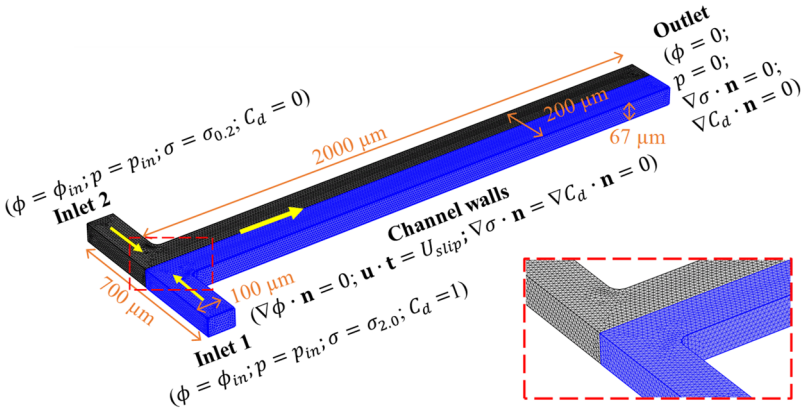

FIG. 3. The meshed computational domain (drawn to scale) of the developed 3D model, where the geometric sizes and boundary conditions (see details in Sec. III B) are highlighted. The inlets 1 and 2 supply the 2.0 mM and 0.2 mM buffer-based PEO solutions, respectively, through the T-shaped microchannel. The block arrows indicate the flow directions. The inset shows a zoom-in view of the tetrahedral meshes at the T-junction.

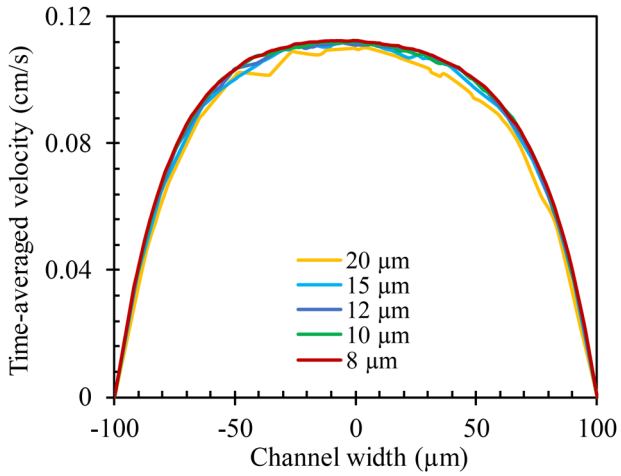

FIG. 4. Comparison of the time-averaged velocity profiles at the cross section 1.5 mm downstream from the T-junction under a 320 V/cm electric field with a range of mesh sizes.

20 μm. Figure 4 compares the corresponding time-averaged velocity profiles at a cross section 1.5 mm downstream from the T-junction under the electric field of 320 V/cm in the main-branch. As no significant differences are viewed between the profiles with the mesh sizes of 8 μm–10 μm, we chose the latter in our simulations to reduce the computation time. Our model was solved in the Palmetto Cluster of Clemson University, and the computation of one case took more than 8 h.

IV. RESULTS AND DISCUSSION

A. Effect of electric field

Figure 5 shows the experimental and numerical images of the fluorescent dye behavior in the electrohydrodynamic coflow of 2.0 mM and 0.2 mM buffer-based PEO solutions. The liquid height difference between the inlet and outlet reservoirs is fixed at 1 cm, while the DC electric field is varied to study the EKI. In the case of 0 ppm PEO in either buffer, for which the system becomes Newtonian fluids with conductivity gradients, similar interfacial electrokinetic behaviors to previous works[14,15] are observed in Fig. 5(a). No EKI waves occur at the T-junction region of the microchannel until the electric field is increased to 350 V/cm (estimated from an applied voltage drop of 630 V across the overall 1.8 cm long channel), which is defined as the threshold electric field, E_{th}. Further increasing the electric field enhances the EKI, where the instability waves become stronger and propagate faster. In contrast, the EKI waves appear in the viscoelastic buffers with 500 ppm PEO at a smaller threshold electric field (E_{th} = 328 V/cm) and take place much closer to the T-junction in Fig. 5(b). Moreover, they are convected downstream at a much lower rate than those in the Newtonian buffers because of the suppressed electroosmotic flow in the PEO solutions. This phenomenon is further demonstrated in Fig. 6 via the time evolution of EKI waves under an identical DC electric field of 389 V/cm. However, the EKI waves in the PEO solutions do not seem to grow significantly stronger with the increase in electric field. The experimentally observed dynamic behaviors of the dye molecules are

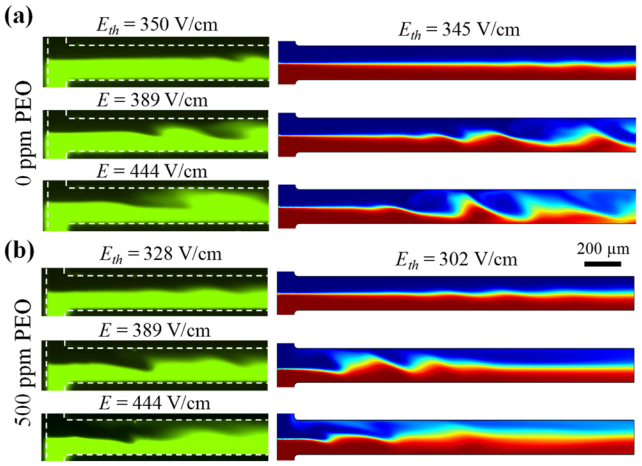

FIG. 5. Experimental images (left column, where the dashed lines highlight the channel walls) and numerical predictions (right column) of the dye concentration in the concurrent electric field- and pressure-driven flow of 2.0 mM (dyed) and 0.2 mM (dye-free) buffer-based PEO solutions through a T-shaped microchannel: (a) 0 ppm PEO (i.e., Newtonian fluids) and (b) 500 ppm PEO (i.e., viscoelastic fluids). The liquid height difference between the inlet and outlet reservoirs is 1 cm in both cases. The values of the applied DC electric field across the microchannel are highlighted above experimental images, where E_{th} is the threshold electric field for the onset of stable EKI waves. The predicted values of E_{th} are also highlighted above the corresponding numerical images. Other values of electric field are identical between the experiment and simulation illustrated in the same row. The highlighted length scale is the same for the experimental and numerical images.

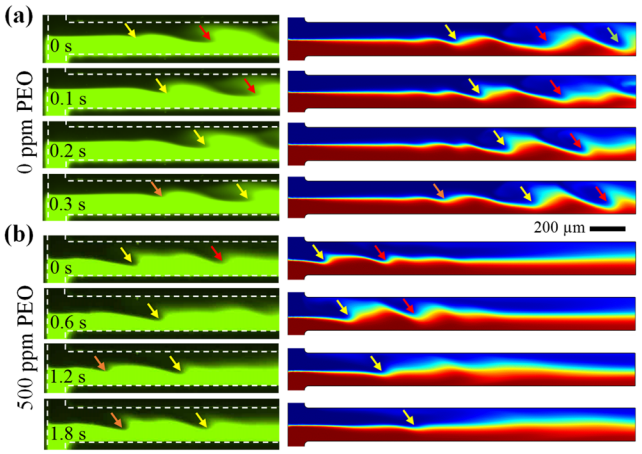

FIG. 6. Experimental images (left column) and numerical predictions (right column) of the dye concentration at different time instants (highlighted on the experimental images) in the concurrent electric field- and pressure-driven coflow of 2.0 mM (dyed) and 0.2 mM (dye-free) buffer-based PEO solutions:(a) 0 ppm PEO and (b) 500 ppm PEO. The liquid height difference between the inlet and outlet reservoirs is 1 cm, and the average DC electric field across the channel is 389 V/cm (above the threshold field) in both cases. The colored arrows highlight the propagation of the EKI waves. The highlighted length scale is the same for the experimental and numerical images.

simulated with a reasonable agreement in both the Newtonian and viscoelastic buffers under varying DC electric fields (Fig. 5) and at different time instants (Fig. 6). However, there are noticeable differences in the observed and predicted locations of the EKI waves, particularly significant in the Newtonian buffer. We attribute this discrepancy to mainly the observation errors in the experimentally measured wall zeta potential and liquid height difference, which affect the computation of the electric field and pressure-driven fluid flows, respectively, in the numerical model and hence the propagation of the EKI waves. A quantitative comparison will be presented in Sec. IV B. It is important to note that our model does not take into account the effect of fluid elasticity on EKI, which may imply that such an effect is actually small as compared to that of the fluid conductivity gradients.

B. Effect of PEO concentration

Figure 7 shows the effect of PEO concentration on the threshold electric field, E_{th}, in the above demonstrated electrohydrodynamic flow of viscoelastic buffer solutions with conductivity gradients. We see from Fig. 7(a) that E_{th} increases at a higher PEO concentration if the liquid height difference between the inlet and outlet reservoirs is fixed. Moreover, E_{th} seems to increase linearly with the imposed liquid height difference (and hence the pressure-driven flow rate) in both the viscoelastic (at any PEO concentrations) and Newtonian buffer solutions. The latter observation is consistent with a recent study from Navaneetham and Posner,[3] which is attributed to the reduced local growth rate of EKI structures at a greater advective velocity. However, the minimum liquid height difference must be increased in order to observe the EKI waves in buffers with a higher PEO concentration. This trend can be well fitted into a 2nd-order polynomial trendline (or an exponential trendline if the data point for the Newtonian buffer, which does not require a complementary pressure-driven flow, is excluded), as illustrated in Fig. 7(b1). A quantitative comparison of the experimentally and numerically obtained E_{th} is presented in Fig. 7(b2) for a fixed 1 cm liquid height difference. The experimental values of E_{th} show a nonmonotonic trend with the PEO concentration, where the decrease from 0 ppm to 250 ppm is mainly a result of the suppressed electroosmotic flow and the continuous increase from 250 ppm to 1000 ppm should be caused primarily by the decreased buffer conductivity ratio (see Fig. 2). They are slightly underpredicted (<10%) by our model for all solutions except that with 1000 ppm PEO (17%). Moreover, the deviation seems to grow with the increase in PEO concentration, which may be because of the neglected fluid elasticity effect that increases with the PEO concentration. Note that our simulations were performed using the experimentally measured conductivity values of the buffer-based PEO solutions in Fig. 2. If the influence of PEO on the buffer conductivity was ignored, the computed E_{th} would become smaller for each PEO concentration because of the greater conductivity ratio than the real value. This would make the numerical curve in Fig. 7(b2) deviates further from the experimental data points.

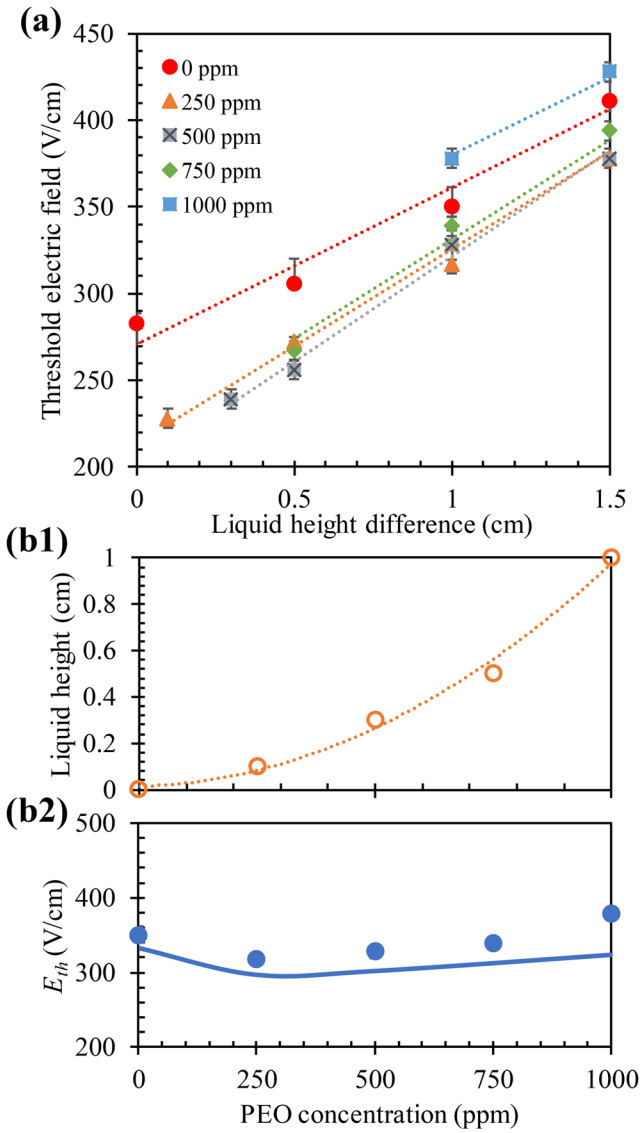

FIG. 7. Threshold electric field, E_{th}, for the onset of EKI in the concurrent electric field and pressure-driven flow of viscoelastic buffer solutions at varying PEO concentrations: (a) experimentally measured values (symbols with error bars and the dotted lines are the linear trendlines of the corresponding experimental data points) of E_{th} in a range of imposed liquid height differences between the inlet and outlet reservoirs; (b1) the minimum liquid height difference (symbols, and the dotted line is the 2nd order polynomial trendline of all the data points) for the onset of EKI increases with the increase in PEO concentration; (b2) comparison of the experimentally measured (symbols) and numerically predicted (solid line) E_{th} under a fixed liquid height difference of 1 cm.

C. Speed and frequency of the EKI waves

We also tracked the "valley" of the EKI waves and determined the wave speed in both the experiment and simulation. In the Newtonian buffer solutions, the measured and predicted wave speeds agree reasonably well and both increase nearly linearly with electric field. This finding, as illustrated in Fig. 8(a), is consistent with that of Chen *et al.*[15] In the viscoelastic buffer solutions, the wave speed becomes much smaller because of the suppressed electroosmotic flow (and hence the overall advective velocity).

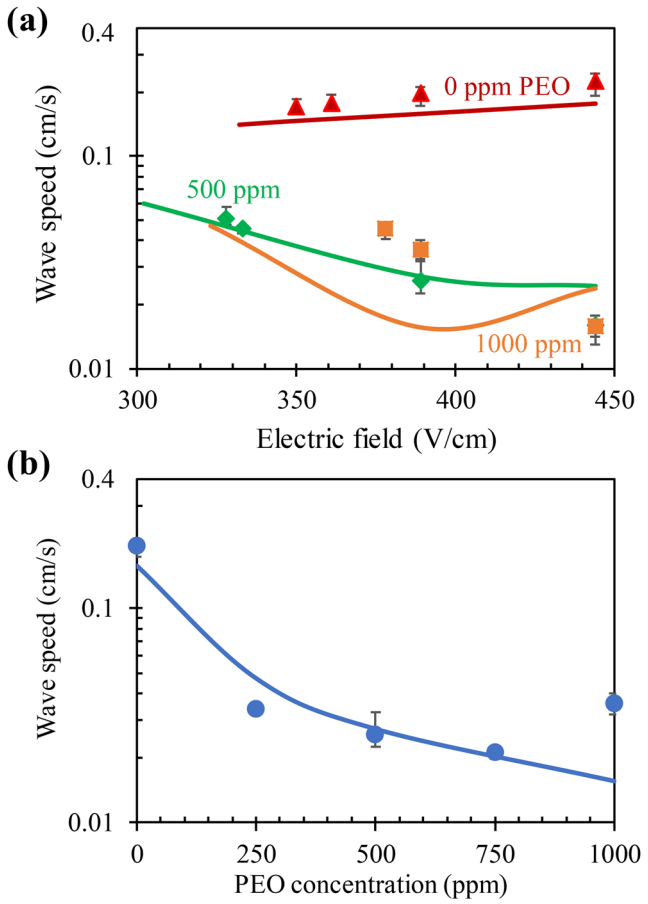

FIG. 8. Experimentally measured (symbols with error bars) and numerically predicted (solid lines) wave speeds for EKI in the concurrent electric field and pressure-driven flow of viscoelastic buffer solutions: (a) wave speed vs DC electric field in buffers of varying PEO concentrations and (b) wave speed vs PEO concentrations under a fixed 389 V/cm DC electric field. The liquid height difference is fixed at 1 cm in all cases.

Surprisingly, it decreases with the increase in electric field in both 500 ppm and 1000 ppm PEO solutions, which may result from the stronger interactions between the EKI waves and the pressure-driven advective flow.[3] Such a trend in 500 ppm PEO is quantitatively predicted by our model, which, however, fails in 1000 ppm PEO likely because of the neglect of the fluid elasticity effect. Figure 8(b) compares the experimentally measured and numerically predicted wave speeds in buffers of varying PEO concentrations under a fixed 389 V/cm DC electric field and a fixed 1 cm liquid height difference. Similar to the observation of E_{th} in Fig. 7(b2), the experimental wave speed also first decreases (from 0 ppm to 750 ppm) and then increases (1000 ppm) with the PEO concentration. This trend might still be the consequence of the competition between the hydrodynamic advective flow and the EKI waves.[3] It agrees well with the numerically predicted curve in Fig. 8(b) except in the 1000 ppm PEO buffers because of the same reason as noted above.

In addition, we did a similar study to Fig. 8 on the temporal frequency of the EKI waves in viscoelastic buffer solutions, which counts the number of occurrences of an instability wave per second at a fixed location of the microchannel. As shown in Fig. 9(a), the frequency of instability waves in the Newtonian buffer solutions first increases and then decreases with the increasing electric field. This trend seems to be reasonably captured by the numerical model and, as explained by Chen *et al.*,[15] may be a result of the transition from convective to absolute instabilities. In contrast, the EKI waves in the viscoelastic buffer solutions have a much lower frequency because of the significantly reduced advective flow therein. Moreover, the wave frequency decreases at higher electric fields in both 500 ppm and 1000 ppm PEO solutions, which may be again a result of the stronger interactions between the EKI waves and the pressure-driven advective flow.[3] Similar to the wave speed in Fig. 8(a), the experimental variation of the wave frequency with electric field is also favorably predicted for 500 ppm PEO but not for 1000 ppm because of the enhanced fluid elasticity effect in the latter. A direct comparison

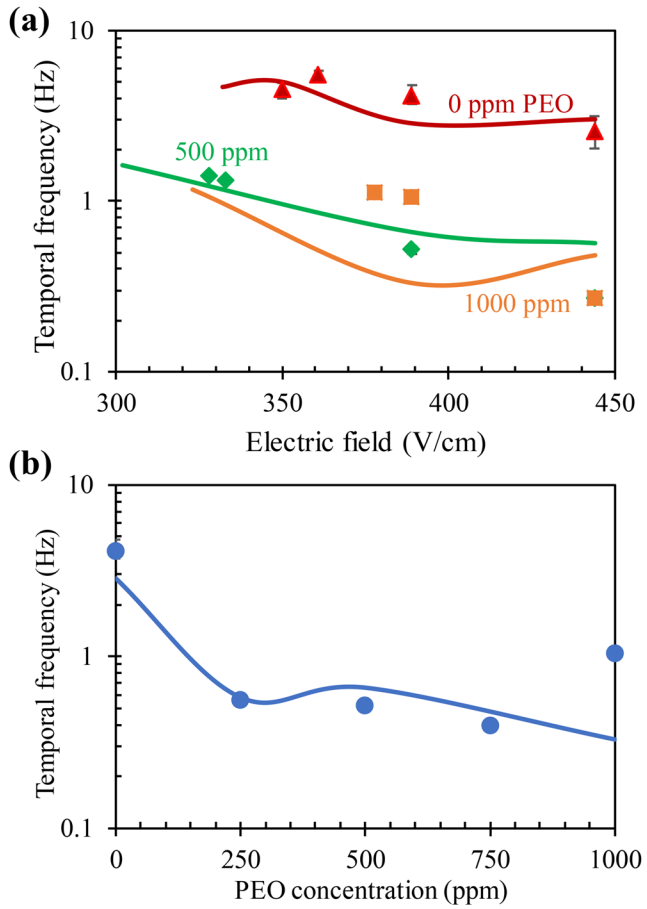

FIG. 9. Experimentally measured (symbols) and numerically predicted (solid lines) temporal frequencies for EKI waves in the concurrent electric field and pressure-driven flow of viscoelastic buffer solutions: (a) temporal frequency vs DC electric field in buffers of varying PEO concentrations and (b) temporal frequency vs PEO concentrations under a fixed 389 V/cm DC electric field. The liquid height difference is fixed at 1 cm in all cases.

of the experimentally and numerically obtained wave frequencies is presented in Fig. 9(b) for a range of PEO concentrations. A similar trend to the wave speed in Fig. 8(b) is observed under both a fixed electric field (389 V/cm) and a fixed liquid height difference (1 cm). Moreover, the numerical prediction deviates from the experimental data point at 1000 ppm PEO because of the neglected fluid elasticity effect.

V. CONCLUSIONS

We have conducted a combined experimental and numerical study of the EKI in coflowing viscoelastic PEO solutions with distinct electric conductivities. The addition of PEO polymer into the Newtonian buffer solutions suppresses the electroosmotic flow, which necessitates the use of a concurrent pressure-driven flow for pumping the viscoelastic solutions. It also alters the conductivity (and in turn the conductivity ratio between the two solutions) and viscosity of the background buffer solutions. These alterations together are found in our experiments to have a significant impact on both the threshold electric field and the EKI waves. Specifically, adding PEO causes first a decrease and then an increase in the threshold electric field for the onset of EKI when the PEO concentration increases. More importantly, adding PEO strongly slows down the propagation speed and reduces the temporal frequency of the EKI waves. To understand the observed dynamic behavior of the dye molecules, we have developed a 3D numerical model in COMSOL that considers such alterations while neglecting the fluid elasticity effect in the buffer-based PEO solutions under a combined electric field and pressure-driven flow. This preliminary model is based on those models available in the literature[22–32] but considers the EKI in a combined electric field and pressure-driven flow. It is found sufficient to capture the electrokinetic flow phenomena at the viscoelastic fluid interface when the PEO solution is within the dilute regime (i.e., ≤750 ppm). The numerical predictions agree quantitatively with the experimental data on the threshold electric field as well as the speed and temporal frequency of the EKI waves. However, the deviation between the numerical and experimental results overall grows with the increase in PEO concentration from 0 ppm to 1000 ppm. This is because the fluid elasticity effect, which increases with the PEO concentration, is neglected in the model. Our findings may imply a smaller effect of the fluid elasticity on EKI than that of the fluid conductivity gradients until the PEO solution becomes semidilute.

Our work represents the first study of the EKI in non-Newtonian fluids. It provides important data to the fundamental understanding of the potential effects of fluid elasticity on EKI. It also provides a useful guide to the design and control of electrokinetic micromixers for non-Newtonian chemical and biological samples in microfluidic applications.[54–57] In future work, we will include the fluid rheological effects (e.g., elasticity and shear thinning) into our model for a more accurate prediction of the EKI in microchannel non-Newtonian fluid flows and further calibrate the revised model using experiments with appropriately selected non-Newtonian fluids.[63]

ACKNOWLEDGMENTS

This work was supported in part by China Scholarship Council (CSC)—Chinese Government Graduate Student Overseas Study Program (L.S.), University 111 Project of China under Grant No. B12019 (L.Y.) and NSF under Grant No. CBET-1704379 (X.X.).

REFERENCES

[1]H. Lin, "Electrokinetic instability in microchannel flows: A review," Mech. Res. Commun. **36**, 33–38 (2009).
[2]J. R. Melcher and G. I. Taylor, "Electrohydrodynamics: A review of the role of interfacial shear stresses," Annu. Rev. Fluid Mech. **1**, 111–146 (1969).
[3]G. Navaneetham and J. D. Posner, "Electrokinetic instabilities of non-dilute colloidal suspensions," J. Fluid Mech. **619**, 331–365 (2009).
[4]L. Ren L, C. Escobedo, and D. Li, "Electroosmotic flow in a microcapillary with one solution displacing another solution," J. Colloid Interface Sci. **242**, 264–271 (2001).
[5]N. T. Nguyen and Z. Wu, "Micromixers: A review," J. Micromech. Microeng. **15**, R1–R16 (2005).
[6]G. Goet, T. Baier, and S. Hardt, "Transport and separation of micron sized particles at isotachophoretic transition zones," Biomicrofluidics **5**, 014109 (2011).
[7]M. A. Saucedo-Espinosa and B. H. Lapizco-Encinas, "Refinement of current monitoring methodology for electroosmotic flow assessment under low ionic strength conditions," Biomicrofluidics **10**, 033104 (2016).
[8]C. C. Chang and R. J. Yang, "Electrokinetic mixing in microfluidic systems," Microfluid. Nanofluid. **3**, 501–525 (2007).
[9]H. Feng, T. N. Wong, Z. Che, and Marcos, "Chaotic micromixer utilizing electro-osmosis and induced charge electro-osmosis in eccentric annulus," Phys. Fluids **28**, 062003 (2016).
[10]S. Azimi, M. Nazari, and Y. Daghighi, "Developing a fast and tunable micromixer using induced vortices around a conductive flexible link," Phys. Fluids **29**, 032004 (2017).
[11]T. Kawamata, M. Yamada, M. Yasuda, and M. Seki, "Continuous and precise particle separation by electroosmotic flow control in microfluidic devices," Electrophoresis **29**, 1423–1430 (2008).
[12]X. Lu, J. P. Hsu, and X. Xuan, "Exploiting the wall-induced non-inertial lift in electrokinetic flow for a continuous particle separation by size," Langmuir **31**, 620–627 (2015).
[13]X. Xuan, "Recent advances in direct current electrokinetic manipulation of particles for microfluidic applications," Electrophoresis (published online 2019).
[14]H. Lin, B. D. Storey, M. H. Oddy, C. Chen, and J. G. Santiago, "Instability of electrokinetic microchannel flows with conductivity gradients," Phys. Fluids **16**, 1922–1935 (2004).
[15]C. Chen, H. Lin, S. K. Lele, and J. G. Santiago, "Convective and absolute electrokinetic instability with conductivity gradients," J. Fluid Mech. **524**, 263–303 (2005).
[16]K. H. Kang, J. Park, I. S. Kang, and K. Y. Huh, "Initial growth of electrohydrodynamic instability of two-layered miscible fluids in T-shaped microchannels," Int. J. Heat Mass Transfer **49**, 4577–4583 (2006).
[17]H. Lin, B. D. Storey, and J. G. Santiago, "A depth-averaged electrokinetic flow model for shallow microchannels," J. Fluid Mech. **608**, 43–70 (2008).
[18]J. D. Posner, C. L. Pérez, and J. G. Santiago, "Electric fields yield chaos in microflows," Proc. Natl. Acad. Sci. U. S. A. **109**, 14353–14356 (2012).
[19]J. Park, S. M. Shin, K. Y. Huh, and I. S. Kang, "Application of electrokinetic instability for enhanced mixing in various micro–T-channel geometries," Phys. Fluids **17**, 118101 (2005).
[20]M. Z. Huang, R. J. Yang, C. H. Tai, C. H. Tsai, and L. M. Fu, "Application of electrokinetic instability flow for enhanced micromixing in cross-shaped microchannel," Biomed. Microdevices **8**, 309–315 (2006).
[21]C. H. Tai, R. J. Yang, M. Z. Huang, C. W. Liu, C. H. Tsai, and L. M. Fu, "Micromixer utilizing electrokinetic instability-induced shedding effect," Electrophoresis **27**, 4982–4990 (2006).
[22]S. M. Shin, I. S. Kang, and Y. K. Cho, "Mixing enhancement by using electrokinetic instability under time-periodic electric field," J. Micromech. Microeng. **15**, 455–462 (2005).
[23]D. A. Boy and B. D. Storey, "Electrohydrodynamic instabilities in microchannels with time periodic forcing," Phys. Rev. E **76**, 026304 (2007).

[24]D. T. Kumar, Y. Zhou, V. Brown, X. Lu, A. Kale, L. Yu, and X. Xuan, "Electric field-driven instabilities in ferrofluid microflows," Microfluid. Nanofluid. **19**, 43 (2015).
[25]L. Song, P. Jagdale, L. Yu, Z. Liu, C. Zhang, R. Gao, and X. Xuan, "Electrokinetic instabilities in co-flowing ferrofluid and buffer solutions with matched electric conductivities," Microfluid. Nanofluid. **22**, 134 (2018).
[26]W. J. Luo, "Effect of ionic concentration on electrokinetic instability in a cross-shaped microchannel," Microfluid. Nanofluid. **6**, 189–202 (2009).
[27]J. D. Posner and J. G. Santiago, "Convective instability of electrokinetic flows in a cross-shaped microchannel," J. Fluid Mech. **555**, 1–42 (2006).
[28]Q. Li, Y. Delorme, and S. H. Frankel, "Parametric numerical study of electrokinetic instability in cross-shaped microchannels," Microfluid. Nanofluid. **20**, 29 (2016).
[29]K. Dubey, A. Gupta, and S. S. Bahga, "Coherent structures in electrokinetic instability with orthogonal conductivity gradient and electric field," Phys. Fluids **29**, 092007 (2017).
[30]B. D. Storey, B. S. Tilley, H. Lin, and J. G. Santiago, "Electrokinetic instabilities in thin microchannels," Phys. Fluids **17**, 018103 (2005).
[31]L. Song, L. Yu, Y. Zhou, A. R. Antao, R. A. Prabhakaran, and X. Xuan, "Electrokinetic instability in microchannel ferrofluid/water co-flows," Sci. Rep. **7**, 46510 (2017).
[32]M. H. Oddy and J. G. Santiago, "Multiple-species model for electrokinetic instability," Phys. Fluids **17**, 064108 (2005).
[33]M. Zehavi, A. Boymelgreen, and G. Yossifon, "Competition between induced-charge electro-osmosis and electrothermal effects at low frequencies around a weakly polarizable microchannel corner," Phys. Rev. Appl. **5**, 044013 (2016).
[34]S. Sánchez, G. Ascanio, F. Méndez, and O. Bautista, "Theoretical analysis of non-linear Joule heating effects on an electroosmotic flow with patterned surface charges," Phys. Fluids **30**, 112002 (2018).
[35]X. Xuan, "Joule heating in electrokinetic flow," Electrophoresis **29**, 33–43 (2008).
[36]R. A. Prabhakaran, Y. Zhou, S. Patel, A. Kale, Y. Song, G. Hu, and X. Xuan, "Joule heating effects on electroosmotic entry flow," Electrophoresis **38**, 572–579 (2017).
[37]A. Kale, L. Song, X. Lu, L. Yu, G. Hu, and X. Xuan, "Electrothermal enrichment of submicron particles in an insulator-based dielectrophoretic microdevice," Electrophoresis **39**, 887–896 (2018).
[38]A. D. Stroock, M. Weck, D. T. Chiu, W. T. S. Huck, P. J. A. Kenis, R. F. Ismagilov, and G. M. Whitesides, "Patterning electro-osmotic flow with patterned surface charge," Phys. Rev. Lett. **84**, 3314 (2000).
[39]U. Ghosh and S. Chakraborty, "Electroosmosis of viscoelastic fluids over charge modulated surfaces in narrow confinements," Phys. Fluids **27**, 062004 (2015).
[40]R. Sarma, N. Deka, K. Sarma, and P. Kumar Mondal, "Electroosmotic flow of Phan-Thien–Tanner fluids at high zeta potentials: An exact analytical solution," Phys. Fluids **30**, 062001 (2018).
[41]U. Ghosh and S. Chakraborty, "Electro-osmosis over inhomogeneously charged surfaces in presence of non-electrostatic ion-ion interactions," Phys. Fluids **28**, 062007 (2016).
[42]E. Biddiss, D. Erickson, and D. Li, "Heterogeneous surface charge enhanced micromixing for electrokinetic flows," Anal. Chem. **76**, 3208–3213 (2004).
[43]C. Y. Lee, G. B. Lee, L. M. Fu, K. H. Lee, and R. J. Yang, "Electrokinetically driven active micro-mixers utilizing zeta potential variation induced by field effect," J. Micromech. Microeng. **14**, 1390–1398 (2004).
[44]S. K. Thamida and H. C. Chang, "Nonlinear electrokinetic ejection and entrainment due to polarization at nearly insulated wedges," Phys. Fluids **14**, 4315 (2002).
[45]G. Yossifon, I. Frankel, and T. Miloh, "On electro-osmotic flows through microchannel junctions," Phys. Fluids **18**, 117108 (2006).
[46]Y. Eckstein, G. Yossifon, A. Seifert, and T. Miloh, "Nonlinear electrokinetic phenomena around nearly insulated sharp tips in microflows," J. Colloid Interface Sci. **338**, 243–249 (2009).
[47]Y. Ren, W. Liu, Z. Wang, and Y. Tao, "Induced-charge electrokinetics in rotating electric fields: A linear asymptotic analysis," Phys. Fluids **30**, 062006 (2018).
[48]J. K. Chen and R. J. Yang, "Vortex generation in electroosmotic flow passing through sharp corners," Microfluid. Nanofluid. **5**, 719–725 (2008).
[49]R. A. Prabhakaran, Y. Zhou, C. Zhao, G. Hu, Y. Song, J. Wang, C. Yang, and X. Xuan, "Induced charge effects on electrokinetic entry flow," Phys. Fluids **29**, 062001 (2017).
[50]Y. Ren, W. Liu, Y. Tao, M. Hui, and Q. Wu, "On AC-field-induced nonlinear electroosmosis next to the sharp corner-field-singularity of leaky dielectric blocks and its application in on-chip micro-mixing," Micromachines **9**, 102 (2018).
[51]C. Y. Lee, C. L. Chang, Y. N. Wang, and L. M. Fu, "Microfluidic mixing: A review," Int. J. Mol. Sci. **12**, 3263–3287 (2011).
[52]M. Zehavi and G. Yossifon, "Particle dynamics and rapid trapping in electro-osmotic flow around a sharp microchannel corner," Phys. Fluids **26**, 082002 (2014).
[53]H. Harrison, X. Lu, S. Patel, C. Thomas, A. Todd, M. Johnson, Y. Raval, T. Tzeng, Y. Song, J. Wang, D. Li, and X. Xuan, "Electrokinetic preconcentration of particles and cells in microfluidic reservoirs," Analyst **140**, 2869–2875 (2015).
[54]A. Lindner, "Flow of complex suspensions," Phys. Fluids **26**, 101307 (2014).
[55]L. L. Ferrás, A. M. Afonso, M. A. Alves, J. M. Nóbrega, and F. T. Pinho, "Electro-osmotic and pressure-driven flow of viscoelastic fluids in microchannels: Analytical and semi-analytical solutions," Phys. Fluids **28**, 093102 (2016).
[56]G. D'Avino, G. Greco, and P. L. Maffettone, "Particle migration due to viscoelasticity of the suspending liquid and its relevance in microfluidic devices," Annu. Rev. Fluid Mech. **49**, 341–360 (2017).
[57]X. Lu, C. Liu, G. Hu, and X. Xuan, "Particle manipulations in non-Newtonian microfluidics: A review," J. Colloid Interface Sci. **500**, 182–201 (2017).
[58]C. Zhao and C. Yang, "Advances in electrokinetics and their applications in micro/nano fluidics," Microfluid. Nanofluid. **13**, 179–203 (2012).
[59]R. J. Poole, M. P. Escudier, A. Afonso, and F. T. Pinho, "Laminar flow of a viscoelastic shear-thinning liquid over a backward-facing step preceded by a gradual contraction," Phys. Fluids **19**, 093101 (2007).
[60]R. M. Bryce and M. R. Freeman, "Extensional instability in electro-osmotic microflows of polymer solutions," Phys. Rev. E **81**, 036328 (2010).
[61]F. Pimenta and M. A. Alves, "Electro-elastic instabilities in cross-shaped microchannels," J. Non-Newtonian Fluid Mech. **259**, 61–77 (2018).
[62]A. Lindner, D. Bonn, and J. Meunier, "Viscous fingering in a shear-thinning fluid," Phys. Fluids **12**, 256–261 (2000).
[63]C. H. Ko, D. Li, A. Malekanfard, Y. N. Wang, L. M. Fu, and X. Xuan, "Electroosmotic flow of non-Newtonian fluids in a constriction microchannel," Electrophoresis **40**, 1387–1394 (2019).
[64]S. J. Haward and G. H. McKinley, "Instabilities in stagnation point flows of polymer solutions," Phys. Fluids **25**, 083104 (2013).
[65]X. Lu, S. Patel, M. Zhang, S. Joo, S. Qian, A. Ogale, and X. Xuan, "An unexpected particle oscillation for electrophoresis in viscoelastic fluids through a microchannel constriction," Biomicrofluidics **8**, 021802 (2014).
[66]X. Lu, J. DuBose, S. Qian, S. Joo, and X. Xuan, "Viscoelastic effects on electrokinetic particle focusing in a constricted microchannel," Biomicrofluidics **9**, 014108 (2015).
[67]D. Li and X. Xuan, "Electrophoretic slip-tuned particle migration in microchannel viscoelastic fluid flows," Phys. Rev. Fluids **3**, 074202 (2018).
[68]A. Malekanfard, C. H. Ko, D. Li, L. Bulloch, A. Baldwin, Y. N. Wang, L. M. Fu, and X. Xuan, "Experimental study of particle electrophoresis in shear-thinning fluids," Phys. Fluids **31**, 022002 (2019).
[69]L. E. Rodd, T. P. Scott, D. V. Boger, J. J. Cooper-White, and G. H. McKinley, "The inertio-elastic planar entry flow of low-viscosity elastic fluids in micro-fabricated geometries," J. Non-Newtonian Fluid Mech. **129**, 1–22 (2005).
[70]X. Lu and X. Xuan, "Elasto-inertial pinched flow fractionation for continuous shape-based particle separation," Anal. Chem. **87**, 11523–11530 (2015).
[71]C. Y. Lim, A. E. Lim, and Y. C. Lam, "Ionic origin of electro-osmotic flow hysteresis," Sci. Rep. **6**, 22329 (2016).
[72]C. Y. Lim, A. E. Lim, and Y. C. Lam, "pH Change in electroosmotic flow hysteresis," Anal. Chem. **89**, 9394–9399 (2017).